Effect of shape and friction on the packing and flow of granular materials

K. Michael Salerno,[1] Dan S. Bolintineanu,[2] Gary S. Grest,[2] Jeremy B. Lechman,[2] Steven J. Plimpton,[2]
Ishan Srivastava,[2] and Leonardo E. Silbert[3]

[1]*U.S. Army Research Laboratory, Aberdeen Proving Ground, Maryland 21005, USA*
[2]*Sandia National Laboratories, Albuquerque, New Mexico 87185, USA*
[3]*School of Math, Science, and Engineering, Central New Mexico Community College, Albuquerque, New Mexico 87106, USA*

The packing and flow of aspherical frictional particles are studied using discrete element simulations. Particles are superballs with shape $|x|^s + |y|^s + |z|^s = 1$ that varies from sphere ($s = 2$) to cube ($s = \infty$), constructed with an overlapping-sphere model. Both packing fraction, ϕ, and coordination number, z, decrease monotonically with microscopic friction μ, for all shapes. However, this decrease is more dramatic for larger s due to a reduction in the fraction of face-face contacts with increasing friction. For flowing grains, the dynamic friction $\tilde{\mu}$—the ratio of shear to normal stresses—depends on shape, microscopic friction, and inertial number I. For all shapes, $\tilde{\mu}$ grows from its quasistatic value $\tilde{\mu}_0$ as $(\tilde{\mu} - \tilde{\mu}_0) = dI^\alpha$, with different universal behavior for frictional and frictionless shapes. For frictionless shapes the exponent $\alpha \approx 0.5$ and prefactor $d \approx 5\tilde{\mu}_0$ while for frictional shapes $\alpha \approx 1$ and d varies only slightly. The results highlight that the flow exponents are universal and are consistent for all the shapes simulated here.

Granular materials are ubiquitous in engineering, industrial, and natural settings. Understanding packing, mechanics, and flow of granular materials like metallic and polymeric powders or rocks and soils is not only of fundamental physical interest but also of important practical concern. Significant advances have been made understanding the nature of granular statics and dynamics through extensive experimental and computational studies of monodisperse spheres [1,2].

It is well established that the microscopic particle friction, μ, strongly influences the stability of static packings of spherical particles, allowing sphere packs to span the density range from random close packing, nominally identified with the packing fraction, $\phi_{\text{rcp}} \approx 0.64$ at $\mu = 0$, down to random loose packing, $\phi_{\text{rlp}} \approx 0.55$ for $\mu \gtrsim 0.5$ [3–9]. Correspondingly, the coordination number z, the average number of contacting particles, also exhibits a continuous decrease from $z_{\text{rcp}} = 6$ to $z_{\text{rlp}} \approx 4$ [4,5,9,10]. From a dynamic view, granular materials similarly express a rich rheology, particularly flows of dense, cohesionless grains [11–13]. Computer simulations continue to prove useful by providing further insight into the rheology of granular materials, especially the role of particle friction [14–16], and by offering ways to test and validate efforts to develop constitutive models [17].

The behavior of aspherical particles is less studied, although it is known that particle shape has an important role in modifying packing [18–28], flow [29–32], and quasistatic mechanical properties [33–37]. At a practical level, most real particulates are frictional and far from spherical, from grains of sand and stones to corn kernels and coffee beans. While shape tends to cause the packing density of frictionless packings to increase with increasing asphericity, at least until the particle aspect ratio exceeds some threshold [38,39], there are some hints that despite differences in shape, frictional nonspherical particles share similarities with spheres [40].

To address the role that particle shape plays in influencing the packing and flow properties of aspherical, frictional materials, we choose a series of particle shapes that can be systematically controlled. One particular class of particle shapes that has received attention are superquadric particles, or superballs [41–46], which are defined by the surface equation:

$$\left| \frac{x}{a} \right|^s + \left| \frac{y}{b} \right|^t + \left| \frac{y}{c} \right|^v = 1. \tag{1}$$

Here, we restrict our study to shapes with $a = b = c$ where a is the characteristic particle length, and to a single shape parameter $s = t = v$. These shapes lie on the spectrum from a sphere of radius a for $s = 2$, to a cube of side $2a$ for $s = \infty$. We study the values $s = 2.0, 2.5, 3.0, 4.5$, and 6.0 that represent the transition from spherical to cubelike shapes, as shown in Fig. 1(a).

Although granular simulations of frictionless aspherical particles is now a well-established technique [24,39,47–59], implementation of the contact mechanics between individual rigid bodies can be cumbersome, especially when tracking static friction forces for the duration that two rigid bodies remain in contact. To overcome contact-detection issues for arbitrarily shaped, composite rigid bodies, we implement a clustered-overlapping sphere algorithm [60] to construct superballs comprised of many component spheres of different sizes. The overlapping-sphere algorithm efficiently packs spheres of variable diameter to fill an arbitrary three-dimensional shape with an algorithm similar to other efforts [53]. Although the overlapped-sphere representation is not perfect, with small gaps between the spheres and surface corrugation relative to the ideal analytic shape, we maintain a balance between the number of spheres used in a shape representation and the fidelity of the representation by using representations that fill at least 95% of the ideal shape volume with as few spheres as possible. For $s = 2.0, 2.5, 3.0, 4.5$,
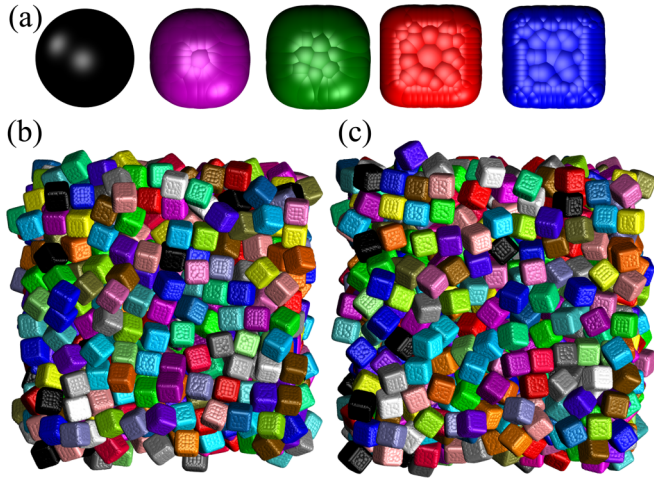
FIG. 1. (a) Superballs created using the overlapping sphere algorithm. From left to right: $s = 2.0$, 2.5, 3.0, 4.5, and 6.0. Bottom: Static packings for $s = 6.0$ superballs with microscopic friction (b) $\mu = 0.0$ and (c) $\mu = 1.0$.

and 6.0, the rigid bodies contain $n = 1$, 163, 71, 179, and 229 spheres, which, respectively, fill 1, 0.9866, 0.9760, 0.9674, and 0.9633 of the ideal superquadric volume. To test the effect of shape fidelity, we also created spheres using $n = 73$ by applying the overlapping-sphere algorithm after placing the first sphere off-center, and a superball with $s = 3.0$ using $n = 125$ spheres. These systems are denoted by $s = 2^*$ and 3^*, respectively, in Fig. 2.

The net force and torque between two contacting rigid bodies are computed from the set of all forces between each pair of contacting spheres that compose the two bodies. Spheres interact via an established linear spring-dashpot contact interaction model [61,62], with normal (n) and tangential (t) forces parametrized by spring constants $k_{n,t}$ and damping factors $\gamma_{n,t}$, respectively. In this work, $k_n = 2k_t = 200\,000$ and $\gamma_n = 2\gamma_t = 33.5\tau^{-1}$, throughout, such that the coefficient
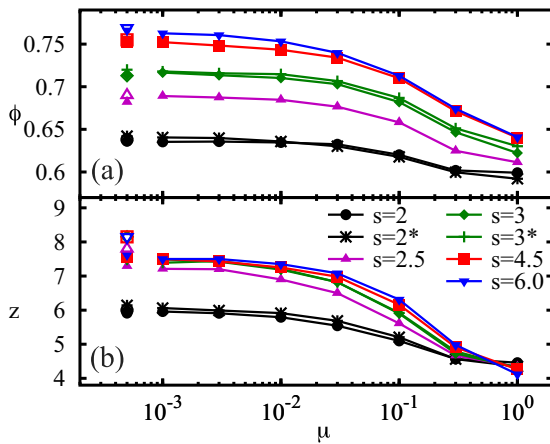

FIG. 2. (a) Packing fraction, ϕ, and (b) coordination number, z, of superball packings over a range in shape parameter, $2 \leqslant s \leqslant 6$, and particle friction coefficient, $0 \leqslant \mu \leqslant 1.0$. Symbols at 5×10^{-4} represent results for $\mu = 0$ (solid) and from Jiao *et al.* [43] (open). The * symbols represent bodies of different fidelity as described in the main text.

of restitution, $e = 0.84$, where time is normalized by the time unit $\tau = \sqrt{m/k_n}$, with m the characteristic mass of a rigid body. The microscopic, sphere friction coefficient, $0 \leqslant \mu \leqslant 1$, represents realistic friction values. All lengths in the simulation are scaled by a, the characteristic length. Particle motion was integrated via the velocity-Verlet algorithm while that of the rigid bodies used the method of quaternions [63] within the open-source LAMMPS software package [64]. The stiffness of the sphere sets the scale for energy and stress, therefore stress and pressure are scaled by k_n/a.

Mechanically stable packings were generated, adapting an isotropic compression protocol with periodic boundary conditions in all three directions [9], close to the limit of marginal stability with a packing pressure $P \approx 10^{-5}$. Figure 2 shows our results on the packing fraction (a) and coordination number (b) as a function of microscopic friction μ over the range $2 < s < 6$. We also use Fig. 2 to illustrate the effectiveness of the overlapping sphere model implemented here by comparing our data to the results of hard-particle, event-driven dynamics simulations of Jiao *et al.* [43] (open symbols) for $\mu = 0$ only. While the fidelity of the overlapping sphere method leads to minor deviations from the "exact" ($\mu = 0$) results, packing fraction values deviate within just a few percent between the different overlapping-sphere representations and the hard-superball simulations [65]. As Fig. 2 displays, superball packings exhibit similar features to spheres: A monotonic decrease in the packing fraction ϕ and coordination number z with increasing μ, for all s. One striking feature is that in the large-μ limit, packings of different shapes tend to converge to a similar state. In other words, the reduction in ϕ and z with μ is more dramatic for larger s, causing frictional superballs with different s to all approach similar values in ϕ and z. Similar to previous studies of frictionless shapes, we also observe that for $s \geqslant 3$ the $\mu = 0$ contact numbers are approximately constant [43]. Indeed, z values for the entire μ range are very similar for $s \geqslant 3$. Our $\mu = 0$ z values lie about 7%–10% below those of Jiao *et al.*, while our values for ϕ are in significantly better agreement [43]. These differences arise from several factors including the computational methodology, the shape interactions (hard vs soft sphere), and especially the overlapping sphere representation, which leads to overly "rounded" shapes and can lead to multiple contacts between pairs of shapes. In particular, the overlapping-sphere representation works to reduce the contact number for a given s value in the jammed state. In contrast, our contact number results for $s = 2$ and $s = 2^*$ agree within 1%–2% with previous results, suggesting that the representation and packing protocol is more important for shapes than for spheres. The change in ϕ with μ and s shown in Fig. 2 arises from the difference in stability of various contact topologies, such as face-face, edge-face, and corner-face, at different friction values, as described below.

From the radial distribution function $g(r)$, shown in Fig. 3(a), there is a distinct shift and broadening of the primary, nearest-neighbor, first peak for $s = 6$ as μ increases, a feature that is absent for spheres [5]. For $\mu = 0$, the nearest-neighbor peak represents face-face contacts which leads to efficient packing. The inset of Fig. 3(a) shows the dramatic decrease in the fraction of particles with at least one face-face contact with increasing μ. While the presence of face-face
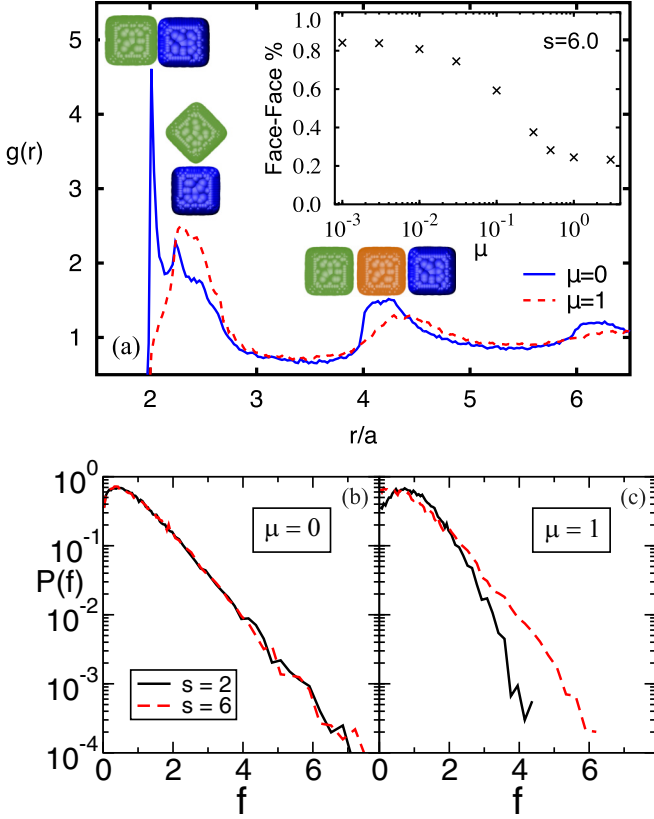
FIG. 3. (a) Radial distribution function, $g(r)$, for $s = 6.0$ with particle friction $\mu = 0.0$ and $\mu = 1.0$. The images reflect likely local structures: face-face, edge-face, and face-face-face, at their respective separations, r. Inset: The fraction of particles for $s = 6.0$ that have at least one face-face contact as a function of the surface friction μ. Bottom: The distribution $P(f)$, of the normalized, normal contact forces f for $s = 2.0$ and $s = 6.0$ packings for (b) $\mu = 0$ and (c) $\mu = 1$.

contacts has been shown to stabilize packings of frictionless Platonic solids [66], for frictional particles other contact topologies such as face-edge contacts become more prevalent. At $\mu = 1.0$, many of these face-face contacts are replaced by local face-edge or face-corner contacts with increasing s, as surmised from the shift of the primary peak in $g(r)$. In addition, the distinctive split in the second peak that is apparent for dense sphere packings is smoothed in the case of superballs, and broadens with increasing friction. As a consequence, these structural dilatational effects cause a decrease in ϕ with increasing s, as all shape packings approach similar values of ϕ and z in the large friction limit. Despite these differences, the distributions of normal contact forces, $P(f)$, shown in Figs. 3(b) and 3(c), where we compare sphere and cube packings, suggest that shape has little effect on the packing mechanical properties for $\mu = 0$, indicating similar behavior to two-dimensional shapes [67]. Whereas, at $\mu = 1$ subtle differences such as enhancement of the large-force tail and an increase in the fraction of smaller forces occur.

We now turn our attention to flow. Our flow results are shown in Figs. 4 and 5. Numerous studies of granular flows [14–17,68–70] have highlighted the influence of microscopic friction on the ratio of the shear stress to the normal stress. It is
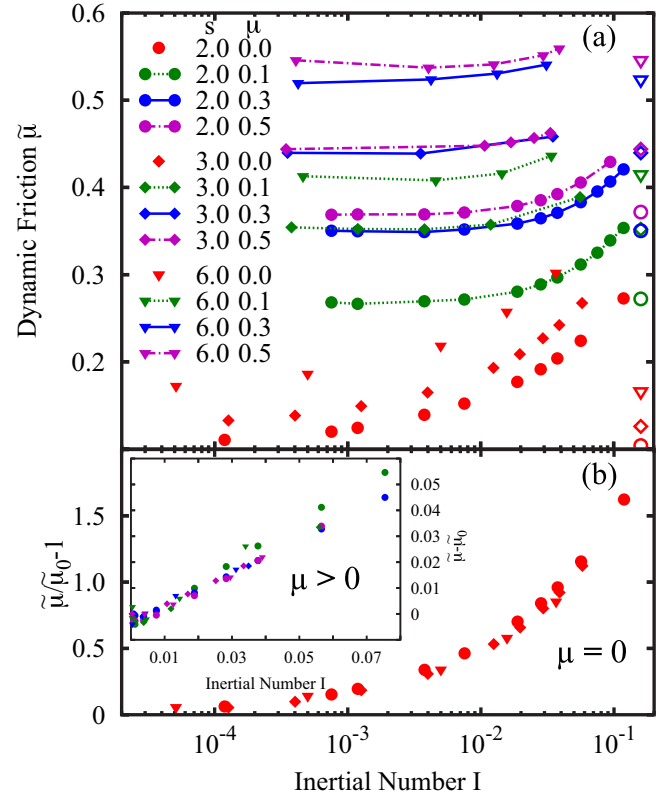

FIG. 4. Rheology curves for flowing superballs with $s = 2.0$, 3.0, and 6.0. (a) Dynamic friction coefficient $\tilde{\mu}$ as a function of the inertial number, I. At small I, all curves approach a constant value. Values of $\tilde{\mu}_0$ used in (b) are indicated by open symbols at $I = 0.16$. (b) The scaled dynamic friction coefficient $\tilde{\mu}/\tilde{\mu}_0 - 1$ for $s = 2.0$, 3.0, and 6.0 at zero friction. Inset: The shifted dynamic friction coefficient $\tilde{\mu} - \tilde{\mu}_0$ for frictional shapes.

useful to think of this ratio as the bulk, macroscopic, *dynamic friction coefficient*, or stress anisotropy, $\tilde{\mu}$. This dynamic friction coefficient scales with inertial number I according to the rheological law,

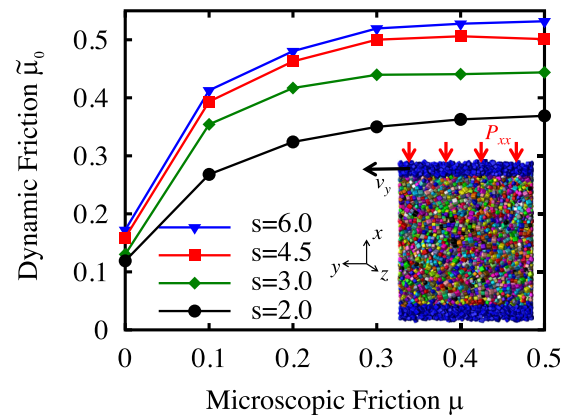$$\tilde{\mu} = \tilde{\mu}_0 + dI^\alpha, \qquad (2)$$

FIG. 5. The dynamic friction coefficient $\tilde{\mu}_0$, in the quasistatic limit ($I \to 0$), as a function of the microscopic friction μ, for shape parameter $s = 2.0$, 3.0, 4.5, and 6.0. Inset: A schematic of the flow sample showing how the wall velocity and pressure are applied.

with $\tilde{\mu}_0$ the value in the quasistatic limit $I \to 0$. The inertial number $I = 2\dot{\gamma}a\sqrt{\rho/P_{xx}}$ is a dimensionless number that depends on the strain rate $\dot{\gamma}$, particle diameter $2a$, particle density ρ, and confining pressure P_{xx}. For spheres, the power-law exponent, α, is distinct for frictionless and frictional particle flows: For $\mu = 0$, $\alpha \approx 0.5$, while for $\mu > 0$, $\alpha \approx 1.0$ [71].

Flowing states contain $N = 6250$ superballs of radius ratio $1 : 1.4$ and number ratio $1.4^3 : 1$ to preserve equal volumes of each species and to avoid ordering during flow. Initially, dilute samples are compressed along the x direction by two rigid walls, with the y and z directions periodic. The sheared system has geometry $L_x \approx 90a$, $L_y = 70a$, $L_z = 10a$, as shown in the inset to Fig. 5. The x position of the upper wall is pressure controlled, according to the equation $\dot{x}_{\text{upp}} = [P(t) - P_{xx}]A/\Gamma$, with damping parameter $\Gamma = 44m/\tau$, the cross-sectional area A, and with a target normal pressure $P_{xx} = 10^{-3}$. Shear flow was imposed by applying a constant y velocity v_{upp} to the top wall. We varied v_{upp} to span a range of dimensionless inertial number I, from rapid flow ($I \approx 0.1$), through the inertial regime, down to the quasistatic limit, $I < 10^{-4}$.

Rheology data over the full range of I shown in Fig. 4(a) show the quantitative dependence of the dynamic friction on shape. The results span a wide range of inertial number I for several values of surface friction μ and shape s. Estimates of the quasistatic friction value $\tilde{\mu}_0$ for each s and μ are shown on the right as open symbols at $I = 0.16$ [72]. We discuss the data for frictionless and frictional shapes separately below.

In Fig. 4(b) the frictionless data are presented. For frictionless particles, we measure that all our data follow the same power law with exponent, $\alpha(\mu = 0) \approx 0.5$, independent of shape. This exponent is slightly larger than previous measurements for spheres, circles, and pentagons [73,74]. We note that we do not determine precise exponents within our data, but rather aim to compare between frictionless and frictional particles. Further, the excellent collapse of $\tilde{\mu}(I)/\tilde{\mu}_0 - 1$ as a function of I implies that $\tilde{\mu}_0$ and d are proportional, and we estimate that $d(\mu = 0) \approx 5\tilde{\mu}_0$. These results indicate the universality of the $\alpha \approx 0.5$ scaling for frictionless particles and that the dynamic friction of frictionless particles is controlled by the quasistatic limit. We note that these results appear independent of how the shapes are represented.

The inset panel of Fig. 4(b) contains data for frictional particles, plotted with the quasistatic value $\tilde{\mu}_0$ subtracted, $\tilde{\mu} - \tilde{\mu}_0$. All data exhibit approximately linear dependence, indicating $\alpha \approx 1$. Also, all the data have a similar slope, suggesting that d is approximately independent of particle shape when microscopic friction is present [75]. The dependence of slope on microscopic friction μ cannot be ruled

out by our data, which is consistent with previous results for frictional flow of disks in two dimensions [16]. We speculate that dimensionality and particle shape may shift the phase diagram proposed previously [16] while maintaining the same qualitative features.

Values of the quasistatic limit of the dynamic friction coefficient $\tilde{\mu}_0$ are shown in Fig. 5 for $s = 2.0, 3.0, 4.5$, and 6.0 over a range of particle microscopic friction μ. The data indicate that $\tilde{\mu}$ monotonically increases with s and μ, saturating at a shape-dependent value at large μ.

In conclusion, we have shown that the static packing fraction and contact number for superball packings depend on shape parameter s and microscopic friction μ, yet follow trends similar to that of spheres. As particles become more aspherical, face-edge and face-corner contacts stabilize at high friction, replacing the face-face contacts that pack more densely. Results show that the rheology of aspherical particles shares similarities with spheres. In particular, the power-law exponent of the I dependence is $\alpha = 0.5$ for frictionless particles and $\alpha = 1.0$ for frictional particles, independent of shape. This result suggests that results previously found in two dimensions extend also to three dimensions [73]. Interestingly, the distinction between $\mu = 0$ and $\mu > 0$ also applies to the quasistatic value of the dynamic friction coefficient $\tilde{\mu}_0$ and the prefactor d with $d \sim \tilde{\mu}_0(s)$ for frictionless particles, and d approximately constant for the frictional shapes simulated here. These results indicate both common and distinct aspects of packing and flow between spherical and aspherical particles. On the one hand, the microscopic properties of grains can be somewhat overlooked when discussing general qualitative behavior, while on the other, specific bulk material properties require a more detailed understanding of the constituent particles.

[1] M. van Hecke, J. Phys.: Condens. Matter **22**, 33101 (2010).

[2] S. Franklin and M. Shattuck, *Handbook of Granular Materials* (CRC Press, Boca Raton, 2016).

[3] S. Torquato, T. M. Truskett, and P. G. Debenedetti, Phys. Rev. Lett. **84**, 2064 (2000).

[4] Z. P. Zhang, L. F. Liu, Y. D. Yuan, and A. B. Yu, Powder Technol. **116**, 23 (2001).

[5] L. E. Silbert, D. Ertaş, G. S. Grest, T. C. Halsey, and D. Levine, Phys. Rev. E **65**, 031304 (2002).

[6] M. Jerkins, M. Schröter, H. L. Swinney, T. J. Senden, M. Saadatfar, and T. Aste, Phys. Rev. Lett. **101**, 018301 (2008).

[7] Y. Jin and H. A. Makse, Physica A **389**, 5362 (2010).

[8] G. Farrell, K. M. Martini, and N. Menon, Soft Matter **6**, 2925 (2010).

[9] L. E. Silbert, Soft Matter **6**, 2918 (2010).

[10] H. P. Zhang and H. A. Makse, Phys. Rev. E **72**, 011301 (2005).

[11] Y. Forterre and O. Pouliquen, Annu. Rev. Fluid Mech. **40**, 1 (2008).

[12] A. Fall, G. Ovarlez, D. Hautemayou, C. Mézière, J.-N. Roux, and F. Chevoir, J. Rheol. **59**, 1065 (2015).

[13] K. A. Gillemot, E. Somfai, and T. Börzsönyi, Soft Matter **13**, 415 (2017).

[14] M. Otsuki and H. Hayakawa, Phys. Rev. E **83**, 051301 (2011).

[15] R. C. Hurley and J. E. Andradé, Granular Matter **17**, 287 (2015).

[16] E. DeGiuli, J. N. McElwaine, and M. Wyart, Phys. Rev. E **94**, 012904 (2016).

[17] K. Kamrin and G. Koval, Comput. Particle Mech. **1**, 169 (2014).

[18] R. Zou and A. Yu, Powder Technol. **88**, 71 (1996).

[19] W. N. Man, A. Donev, F. H. Stillinger, M. T. Sullivan, W. B. Russel, D. Heeger, S. Inati, S. Torquato, and P. M. Chaikin, Phys. Rev. Lett. **94**, 198001 (2005).

[20] K. Desmond and S. V. Franklin, Phys. Rev. E **73**, 031306 (2006).

[21] J. Blouwolff and S. Fraden, Europhys. Lett. **76**, 1095 (2006).

[22] A. Jaoshvili, A. Esakia, M. Porrati, and P. M. Chaikin, Phys. Rev. Lett. **104**, 185501 (2010).

[23] A. G. Athanassiadis, M. Z. Miskin, P. Kaplan, N. Rodenberg, S. H. Lee, J. Merritt, E. Brown, J. Amend, H. Lipson, and H. M. Jaeger, Soft Matter **10**, 48 (2014).

[24] K. C. Smith, I. Srivastava, T. S. Fisher, and M. Alam, Phys. Rev. E **89**, 042203 (2014).

[25] L. K. Roth and H. M. Jaeger, Soft Matter **12**, 1107 (2016).

[26] L. Meng, Y. Jiao, and S. Li, Powder Technol. **292**, 176 (2016).

[27] H. Malmir, M. Sahimi, and M. R. Rahimi Tabar, Phys. Rev. E **95**, 052902 (2017).

[28] S. Zhao, N. Zhang, X. Zhou, and L. Zhang, Powder Technol. **310**, 175 (2017).

[29] T. Börzsönyi and R. E. Ecke, Phys. Rev. E **76**, 031301 (2007).

[30] T. Börzsönyi and R. Stannarius, Soft Matter **9**, 7401 (2013).

[31] S. Wegner, R. Stannarius, A. Boese, G. Rose, B. Szabó, E. Somfai, and T. Börzsönyi, Soft Matter **10**, 5157 (2014).

[32] C. D. Cwalina, K. J. Harrison, and N. J. Wagner, Soft Matter **12**, 4654 (2016).

[33] E. Azéma, N. Estrada, and F. Radjaï, Phys. Rev. E **86**, 041301 (2012).

[34] E. Azéma, F. Radjaï, B. Saint-Cyr, J.-Y. Delenne, and P. Sornay, Phys. Rev. E **87**, 052205 (2013).

[35] E. Azéma, F. Radjaï, R. Peyroux, and G. Saussine, Phys. Rev. E **76**, 011301 (2007).

[36] M. Boton, E. Azéma, N. Estrada, F. Radjaï, and A. Lizcano, Phys. Rev. E **87**, 032206 (2013).

[37] E. Azéma, F. Radjai, and G. Saussine, Mech. Mater. **41**, 729 (2009).

[38] A. Donev, R. Connelly, F. H. Stillinger, and S. Torquato, Phys. Rev. E **75**, 051304 (2007).

[39] C. F. Schreck, N. Xu, and C. S. O'Hern, Soft Matter **6**, 2960 (2010).

[40] J. Baker and A. Kudrolli, Phys. Rev. E **82**, 061304 (2010).

[41] P. W. Cleary and M. L. Sawley, Appl. Math. Model. **26**, 89 (2002).

[42] Y. Jiao, F. H. Stillinger, and S. Torquato, Phys. Rev. E **79**, 041309 (2009).

[43] Y. Jiao, F. H. Stillinger, and S. Torquato, Phys. Rev. E **81**, 041304 (2010).

[44] R. D. Batten, F. H. Stillinger, and S. Torquato, Phys. Rev. E **81**, 061105 (2010).

[45] J. R. Royer, G. L. Burton, D. L. Blair, and S. D. Hudson, Soft Matter **11**, 5656 (2015).

[46] D. J. Audus, A. M. Hassan, E. J. Garboczi, and J. F. Douglas, Soft Matter **11**, 3360 (2015).

[47] G. T. Nolan and P. E. Kavanagh, Powder Technol. **84**, 199 (1995).

[48] A. Džiugys and B. Peters, Granular Matter **3**, 231 (2001).

[49] P. A. Langston, M. A. Al-Awamleh, F. Y. Fraige, and B. N. Asmar, Chem. Eng. Sci. **59**, 425 (2004).

[50] A. Wouterse, S. R. Williams, and A. P. Philipse, J. Phys.: Condens. Matter **19**, 406215 (2007).

[51] J. Hilton, L. Mason, and P. Cleary, Chem. Eng. Sci. **65**, 1584 (2010).

[52] S. Abedi and A. Mirghasemi, Particuology **9**, 387 (2011).

[53] C. L. Phillips, J. A. Anderson, G. Huber, and S. C. Glotzer, Phys. Rev. Lett. **108**, 198304 (2012).

[54] E. Azéma, Y. Descantes, N. Roquet, J.-N. Roux, and F. Chevoir, Phys. Rev. E **86**, 031303 (2012).

[55] D. Höhner, S. Wirtz, and V. Scherer, Powder Technol. **226**, 16 (2012).

[56] Y. Guo, C. Wassgren, B. Hancock, W. Ketterhagen, and J. Curtis, Phys. Fluids **25**, 063304 (2013).

[57] J. Katagiri, T. Matsushima, and Y. Yamada, Granular Matter **16**, 891 (2014).

[58] K. Dong, C. Wang, and A. Yu, Chem. Eng. Sci. **126**, 500 (2015).

[59] T. Zhao, F. Dai, N. W. Xu, Y. Liu, and Y. Xu, Granular Matter **17**, 763 (2015).

[60] X. Garcia, J.-P. Latham, J. Xiang, and J. Harrison, Géotechnique **59**, 779 (2009).

[61] P. A. Cundall and O. D. L. Strack, Géotechnique **29**, 47 (1979).

[62] L. E. Silbert, D. Ertaş, G. S. Grest, T. C. Halsey, D. Levine, and S. J. Plimpton, Phys. Rev. E **64**, 051302 (2001).

[63] P. Allen and D. Tildesley, *Computer Simulation of Liquids*, Oxford Science Publications (Clarendon, Oxford, 1989).

[64] S. Plimpton, J. Comput. Phys. **117**, 1 (1995).

[65] Due to the approximate superball representation of the overlapping-sphere model, the packing fraction values given in Fig. 2 have been corrected to account for the volume occupied by 1000 *ideal* superballs.

[66] K. C. Smith, T. S. Fisher, and M. Alam, Phys. Rev. E **84**, 030301 (2011).

[67] B. Saint-Cyr, J.-Y. Delenne, C. Voivret, F. Radjai, and P. Sornay, Phys. Rev. E **84**, 041302 (2011).

[68] C. S. Campbell, J. Fluid Mech. **465**, 261 (2002).

[69] F. da Cruz, S. Emam, M. Prochnow, J.-N. Roux, and F. Chevoir, Phys. Rev. E **72**, 021309 (2005).

[70] T. Guo and C. S. Campbell, Phys. Fluids **28**, 083303 (2016).

[71] M. Bouzid, A. Izzet, M. Trulsson, E. Clément, P. Claudin, and B. Andreotti, Eur. Phys. J. E **38**, 125 (2015).

[72] Quasistatic dynamic friction values were determined in two ways: For frictional data, a linear fit was used on the rheology data to determine the intercept $\tilde{\mu}_0$, which agreed with the lowest measured dynamic friction values $\tilde{\mu}(I \rightarrow 0)$, to within 1.5%. For frictionless particles quasistatic values are chosen to eliminate curvature at small I when data are plotted on log-log axes.

[73] É. Azéma, F. Radjaï, and J.-N. Roux, Eur. Phys. J. E **41**, 2 (2018).

[74] P.-E. Peyneau and J.-N. Roux, Phys. Rev. E **78**, 011307 (2008).

[75] Plotting $\tilde{\mu}(I)/\tilde{\mu}_0 - 1$ for the $\mu > 0$ data gives a poor collapse.